Tailoring enhanced optical chirality – design principles for chiral plasmonic nanostructures

Martin Schäferling Daniel Dregely Mario Hentschel
Harald Giessen

– Supplementary Information –

1 Dissymmetry factor g^*

We consider the two enantiomers of a chiral plasmonic structure. Then the interaction with circularly polarized light depends on the handedness of the structure and the polarization of the incident light. We start with the distributions $U_{e,1}^{+}\left(\vec{r}\right)$ and $C_1^{+}\left(\vec{r}\right)$ of electric energy density and optical chirality for the left-handed enantiomer and left-handed circularly polarized light. When changing the incident polarization, the response changes in a complicated way due to the different interaction of the incident field with the plasmonic structure. However, for each spatial position $\vec{r}$ we can find a location $\vec{r'}$ where the near-field of the second enantiomer generated by incident right-handed circularly polarized light shows the same electric field density and opposite optical chirality. $\vec{r}$ and $\vec{r'}$ are correlated by the same mirror operation which translates the two enantiomers one into another:

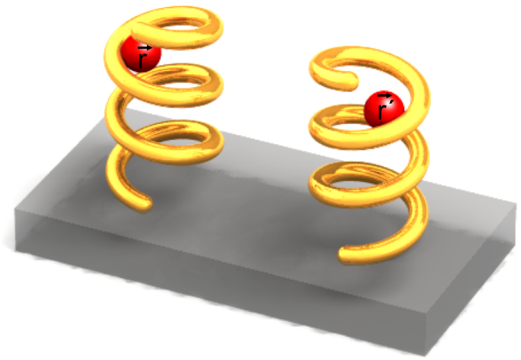

This leads to the relations

$$U_{e,1}^{+}\left(\vec{r}\right) = U_{e,2}^{-}\left(\vec{r'}\right) , \qquad C_1^{+}\left(\vec{r}\right) = -C_2^{-}\left(\vec{r'}\right) ,$$
$$U_{e,2}^{+}\left(\vec{r}\right) = U_{e,1}^{-}\left(\vec{r'}\right) , \qquad C_2^{+}\left(\vec{r}\right) = -C_1^{-}\left(\vec{r'}\right) .$$

We now consider two molecules located at $\vec{r}$ and $\vec{r'}$, respectively. Their combined excitation A^* for the different polarizations can be quantified via

$$A^{*,\pm} = A_1^{\pm} + A_2^{\pm} \propto \alpha\omega\left(U_{e,1}^{\pm} + U_{e,2}^{\pm}\right) - \beta\left(C_1^{\pm} + C_2^{\pm}\right) = \alpha\omega\left(U_{e,1}^{\pm} + U_{e,1}^{\mp}\right) - \beta\left(C_1^{\pm} - C_1^{\mp}\right)$$

using Eq. (2) from the manuscript and the relations developed before. By analogy with the definition of the dissymmetry factor (cf. Eq. (5) in the manuscript) we can define a dissymmetry factor g^* for this combined system:

$$g^* := \frac{2\left(A^{*,+} - A^{*,-}\right)}{A^{*,+} + A^{*,-}} \propto -\frac{C_1^+ - C_1^-}{U_{e,1}^+ + U_{e,1}^-}\,.$$

Therefore, it is sufficient to calculate the electromagnetic response of only one enantiomer to obtain g^*. Using the relations between the fields of the enantiomers we can calculate this dissymmetry factor using the second enantiomer:

$$g^* \propto -\frac{C_2^- - C_2^+}{U_{e,2}^+ + U_{e,2}^-}\,.$$

The numeration of the two enantiomers is arbitrary. Change of the numeration would lead to a sign flip in g^*. For convenience, we decided to label the left-handed enantiomer as 1. For circularly polarized light without any chiral nanostructure we end up with $g \propto -C/U_e$ which is the result of [22].

Please note that this describes not the enantioselectivity at one single point in space but the combined value for two molecules located at symmetric positions near enantiomeric plasmonic nanostructures. For a quantitiative analysis, one should integrate over the whole space covered with chiral molecules. Nevertheless, this value suits for a comparison to experiments using only circularly polarized light. Similar to the enhancement $\hat{C}$ of optical chirality one can calculate the enhancement of the dissymmetry factor as

$$\hat{g}^* := \frac{g^*}{g_{\mathrm{CPL}}} = g^* \cdot \frac{U_e}{C}\,.$$

An alternative would be to calculate g from $U_e^\pm$ and $C^\pm$ directly using Eqs. (2) and (5) from the manuscript. Unfortunately, this requires to use specific values for α and β which lowers the comparability. Additionally, the calculation of $A^\pm$ is numerically challenging as the values of $C^\pm$ are several orders of magnitude smaller than those of $U_e^\pm$. This requires high accuracy in the numerical calculation of these values.

2 Simulation environment

We used the commercially available software CST Microwave Studio for the simulations, which implements a frequency-domain finite element solver for Maxwell's equations. We modeled an infinite two-dimensional array of the different structures, which were embedded in air. Tab. 1 stores the dimensions of the unit cells for the different structures. The gold was modeled using a Drude model with a plasma frequency of $1.37 \times 10^{16}\,\mathrm{s}^{-1}$ and a collision frequency of $1.22 \times 10^{14}\,\mathrm{s}^{-1}$.

For each structure, an iteration of adaptive mesh refinement steps was performed until the difference in the results for subsequent steps was below 0.01. The number of cells in the resulting mesh is also shown in Tab. 1. Each field calculation was iterated until a relative residual norm below 10^{-4} was reached. To calculate the spectra, which were used to decide for

the frequencies were the optical activity was calculated, CST chooses the frequency samples adaptively and interpolates the spectra. The error estimate (for all scattering parameters) is also given in Tab. 1.

Table 1: Details about the simulation for the six structures.

Structure	**Unit cell (nm x nm)**	**Mesh cells x1000**	**Error estimate**
Helix (left)	750×750	189	4×10^{-3}
Helix (right)	750×750	189	4×10^{-3}
Gammadion	800×800	22	2×10^{-4}
Spiral	1100×1100	31	2×10^{-3}
Oligomer	650×650	45	9×10^{-5}
Stereometamaterial	700×700	27	4×10^{-4}

Note that CST uses the source view convention for defining the handedness of the polarization states. We ensured that for all our simulations the given handedness confirms with the handedness of the helix the field vectors constitute in space at a fixed time. This is crucial when comparing the polarizations with the handedness of a structure, which is defined in a similar way.

The optical chirality was calculated in MATLAB from the electric and magnetic fields provided by CST. To obtain the enhancement, we normalized the calculated values with the optical chirality of circularly polarized light without any structure at the same frequency.

Although the residual norm was choosen to be below 10^{-4}, errors can occur at the sharp interfaces. These led to single points with erroneously high values for the optical chirality in our simulations (e. g., values more than twice as high than any of the direct neighbors). We used a $3 \times 3 \times 3$ median filter to remove this numerical noise. This is a simple and powerful technique to deal with that sort of error.

All calculations were performed on standard desktop hardware, only for the helix a multi CPU machine has been used. The computing time depends strongly on the number of mesh cells. Basically, every structure could be simulated within several hours on that kind of hardware.

3 Visualization

We used POVRay to visualize our results. The volume rendering was obtained by a transparent medium whose density and color was influenced by the local value of the optical chirality. Due to the transparency the color of one distinct point depends not only on the actual optical chirality value at this point but also on the color of the region behind. Please refer to the two-dimensional slices to obtain quantitative insights.

All three-dimensional plots feature the same colormap which allows a direct comparison of the different structures. Absolute values below 2.5 were set fully transparent, as these values are in the range of the chirality difference of circularly polarized light. Therefore, dismissing these values is no lack of information, but allows for an easier identification of regions with high optical chirality.

4 Structure comparison

Table 2 shows the extracted data for the minimum and maximum chirality enhancement for all discussed structures after the filtering process. Please note that these numbers allow only a rough comparison as it is also important to have continuous and homogeneous regions with enhanced chirality. Additionally, even after the filtering process we can not guarantee that we eliminated all numerical noise. Nevertheless, these values are handy for ranking the structures. Especially the difference value allows some additional insights. With these values one can predict that the gammadion behaves very similar for both polarizations, as the difference is overall very small. As another example, one can infer that the strongest enhancement in the chiral oligomer appears at similar spation positions, but with different signs for the two incident polarizations.

We also show in this table the frequency at which we calculated the optical chirality as well as the corresponding wavelengths. For the gammadion, we took the fundamental plasmonic resonance, as this structure exhibits neither a difference in the circular polarization conversion nor circular dichroism. For the spiral, we took the maximum circular polarization conversion difference, while for all three-dimensional structures the frequency with the maximum circular dichroism was used.

Table 2: Frequencies and extracted maximum and minimum chirality enhancement for the six structures.

Structure	**f (THz)**	**λ (µm)**	**LCP**	**RCP**	**LCP – RCP**
Helix (left)	147.5	2.03	-15 – 23	-4 – 1	-15 – 27
Helix (right)	147.5	2.03	-1 – 4	-24 – 15	-15 – 27
Gammadion	149.5	2.01	-21 – 22	-22 – 21	-3 – 4
Spiral	162.5	1.84	-21 – 30	-28 – 21	-22 – 27
Oligomer	333.0	0.90	-55 – 88	-24 – 4	-51 – 112
Stereometamaterial	223.5	1.34	-13 – 15	-37 – 54	-58 – 36